JARO 17: 525–540 (2016)
DOI: 10.1007/s10162-016-0585-5

JARO
Journal of the Association for Research in Otolaryngology

Research Article

BODIPY-Conjugated Xyloside Primes Fluorescent Glycosaminoglycans in the Inner Ear of *Opsanus tau*

Holly A. Holman,[1] Vy M. Tran,[2] Mausam Kalita,[2] Lynn N. Nguyen,[1] Sailaja Arungundram,[2] Balagurunathan Kuberan,[1,2,3] and Richard D. Rabbitt[1,3,4,5]

[1]*Department of Bioengineering, University of Utah, 36 South Wasatch Dr., Sorenson Molecular Biotechnology Building, Salt Lake City, UT 84112, USA*

[2]*Department of Medicinal Chemistry, University of Utah, 30 South 2000 East, 1972 Skaggs Hall, Salt Lake City, UT 84112, USA*

[3]*Graduate Program in Neuroscience, University of Utah, Salt Lake City, UT 84112, USA*

[4]*Department of Otolaryngology-Head and Neck Surgery, University of Utah, Salt lake City, UT 84112, USA*

[5]*Marine Biological Laboratory, 7 MBL Street, Woods Hole, MA 02543, USA*

Received: 10 April 2016; Accepted: 23 August 2016; Online publication: 12 September 2016

ABSTRACT

We report on a new xyloside conjugated to BODIPY, BX and its utility to prime fluorescent glycosaminoglycans (BX-GAGs) within the inner ear in vivo. When BX is administered directly into the endolymphatic space of the oyster toadfish (*Opsanus tau*) inner ear, fluorescent BX-GAGs are primed and become visible in the sensory epithelia of the semicircular canals, utricle, and saccule. Confocal and 2-photon microscopy of vestibular organs fixed 4 h following BX treatment, reveal BX-GAGs constituting glycocalyces that envelop hair cell kinocilium, nerve fibers, and capillaries. In the presence of GAG-specific enzymes, the BX-GAG signals are diminished, suggesting that chondroitin sulfates are the primary GAGs primed by BX. Results are consistent with similar click-xylosides in CHO cell lines, where the xyloside enters the Golgi and preferentially initiates chondroitin sulfate B production. Introduction of BX produces a temporary block of hair cell mechanoelectrical transduction (MET) currents in the crista, reduction in background discharge rate of afferent neurons, and a reduction in sensitivity to physiological stimulation. A six-degree-of-freedom pharmacokinetic mathematical model has been applied to interpret the time course and spatial distribution of BX and BX-GAGs. Results demonstrate a new optical approach to study GAG biology in the inner ear, for tracking synthesis and localization in real time.

Keywords: BODIPY-xyloside, glycocalyx, glycosaminoglycans, mechanoelectrical transduction

INTRODUCTION

Glycosaminoglycans are essential for the development and function of the nervous system including the inner ear; however, elucidation of their structure and physiological function in vivo has been difficult due to limited molecular tools, minute abundance, and their biochemical properties (Kleene and Schachner, 2004; Matani et al., 2007; Huang and Godula, 2014). When the inner ear sensory organs have altered glycobiology, the result can affect hearing and balance (Gil-Loyzaga et al., 1985; Takumida et al., 1989c; Takumida et al., 1989b; Takumida et al., 1989a; Takumida, 2001). Evidence of GAG-related glycoconjugates, glycocalyces, and structures in the inner ear first appeared in the mid-twentieth century (reviewed by (Go et al. 2011). Dohlman (1971)

Electronic supplementary material The online version of this article (doi:10.1007/s10162-016-0585-5) contains supplementary material, which is available to authorized users.

Correspondence to: Holly A. Holman · Department of Bioengineering · University of Utah · 36 South Wasatch Dr., Sorenson Molecular Biotechnology Building, Salt Lake City, UT 84112, USA. Telephone: 801-587-7241; email: holly.holman@utah.edu

reported electron microscopy studies describing a veil, which stained positive for mucopolysaccharides. This veil was identified in the organ of corti surrounding stereocilia hair bundles and extending to the tectorial membrane. It was also observed in the crista ampullaris, encasing hair cell microvilli in what was thought to be providing a tether to the cupula. To delineate the carbohydrate composition, Suzuki et al. conducted chemical analyses of the utricle glycocalyx and demonstrated the presence of N-linked-glycoconjugates, including keratan sulfates and O-glycosides along with chondroitin sulfates (Sugiyama et al., 1991a; Suzuki et al., 1996). Further studies have shown multiple GAG species, based upon core disaccharide structures, including heparan sulfate (HS), chondroitin sulfate (CS)/dermatan sulfate (DS), keratan sulfate (KS), and hyaluronic acid (HA) in the inner ear. For example, KS has been observed in the subepithelial layer of the utricle and associating with vestibular hair cells, nerve fibers, the otoconial membrane, stria vascularis, and organ of corti (Sugiyama et al. 1991b, a; Katori et al. 1996). While many GAGs are ubiquitously distributed, some GAGs have unique extra cellular matric (ECM) patterns, including HA which localizes to the surface of sensory cells and stereocilia of hair cells, whereas HS has been observed on spiral ganglion and Reissner's membrane (Torihara et al., 1995; Tsuprun and Santi, 2001). Previous data suggests GAGs could be important ECM molecules for anchoring proteoglycans on hair bundles and moving in response to sound and motion (Hultcrantz and Bagger-Sjoback 1996; LeBoeuf et al. 2011). In this case, disruption of GAG synthesis or remodeling could alter hair bundle movement and mechanoelectrical transduction (MET) currents. There is also evidence that GAGs play an important role at synapses and, when altered, can result in impaired short-term plasticity and transmission (Albiñana et al., 2015; Kochlamazashvili et al., 2010; Chicoine et al., 2004; Frischknecht et al., 2009). Here, we describe a new fluorescently conjugated xyloside, BODIPY-xyloside (BX), developed to study the turnover and impact of primed GAGs in the physiology of the inner ear vestibular organs.

Normal priming of GAGs occurs by xylosylation of a serine residue to a core protein. GAGs are synthesized in the Golgi, where core proteins from rER are posttranslationally modified with O-linked glycosylations. GAGs can also be primed using synthetic xylosides without a core protein (Okayama et al., 1973; Schwartz et al., 1974). Synthetic xylosides can compete with endogenous core protein acceptor sites for assembly of GAG chains in the Golgi (Saliba et al., 2015; Nguyen et al., 2013; Weinstein et al., 2012) and thereby provide a tool to perturb GAGs and to examine physiology of inner ear sensory organs. In the present work, BX was designed as a β-D-xyloside, containing a beta linkage of xylose to a hydrophobic aglycone using "click chemistry" (Kuberan et al., 2008). We hypothesized that BX introduced into the endolymph in vivo would enter hair cells and supporting cells to prime the production of fluorescent GAGs (BX-GAGs). The results demonstrate the use of BX as a molecular tool to examine the structure, function, spatial distribution, and turnover of primed GAGs in the inner ear.

METHODS

General Synthetic Procedures of Xylosides

Xylosides were synthesized using methods previously reported (Kuberan et al., 2008; Tran et al., 2010; Nguyen et al., 2013). Briefly, all chemical reactions were performed under nitrogen atmosphere with oven-dried glassware using standard techniques. Anhydrous solvents were dried and freshly distilled immediately prior to their use. All synthetic compounds were characterized by (^{1}H) and carbon (^{13}C) NMR spectra obtained on a Bruker 400-MHz spectrometer. Chemical shifts were relative to the deuterated solvent peak or the tetramethylsilane (TMS) peak at (δ 0.00) and are in parts per million (ppm). High-resolution mass spectrometry (HRMS) was performed using a Finnigan LCQ mass spectrometer in either positive or negative ion mode. Thin layer chromatography (TLC) was done on 0.25 mm thick precoated silica gel HF_{254} aluminum sheets. Chromatograms were observed under short and long wavelength UV light and visualized by heating plates that were dipped in a solution of Von's reagent containing ammonium (VI) molybdate tetrahydrate (12.5 g) and cerium (IV) sulfate tetrahydrate (5.0 g) in 10 % aqueous sulfuric acid (500 ml). Flash column chromatography was performed using silica gel 60 (230–400 mesh) and employed a stepwise solvent polarity gradient, correlated with TLC mobility and were run under pressure of 5–7 psi. HPLC was used to purify the final products using a C18 column (VYDAC 2.2 cm × 25 cm) with solvent A (25 mM formic acid) and solvent B (95 % acetonitrile) at a flow rate of 5 ml/min in a linear gradient over 120 min starting with 0 % B.

Fluorescent Conjugated Xyloside Synthesis (Fig. 1A)

Compound 1

4-Hydroxyl benzaldehydes (1 mmol) and pyrrole (10 mmol) were added to a round bottom flask and

degassed with argon for 5 min, followed by the addition of trifluoroacetic acid (0.1 ml). Condensation of 4-substituted benzaldehydes with pyrrole formed dipyrromethane, which was stirred under argon at room temperature for 1 h, and the excess pyrrole was subsequently removed. The reaction mixture was then evaporated under vacuum to give a residue that was further purified by low pressure flash silica column chromatography to yield the known compound 1 (Fig. 1A (1)).

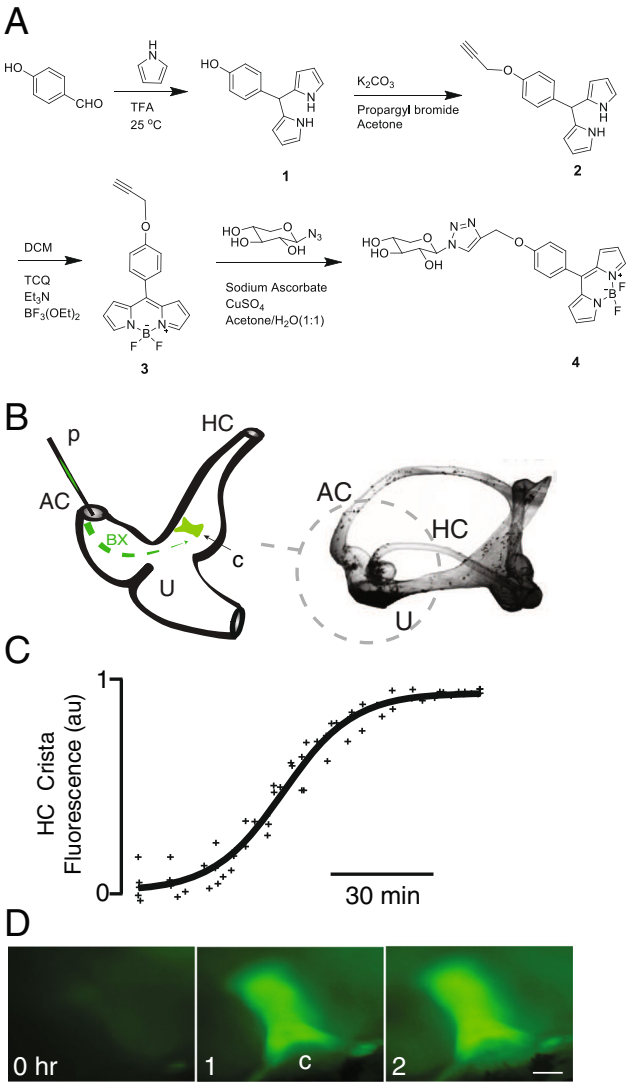

FIG. 1. BODIPY-xyloside (BX) synthesis and its application in the *Opsanus tau* vestibular system. **A** Schematic representation of the BX synthesis with its chemical structures in a four-step process, with intermediate structures provided (*1–3*). **B** Cartoon illustrating in vivo delivery of BX loaded into a pulled glass micropipette (*p*) and mixed with the endolymph and delivered via a fenestration into the dorsal course of the anterior canal (*AC*). , BX-GAGs fluorescently labeled regions of the horizontal canal (*HC*), crista (*c*) increased to a maximum intensity within 2 h postadministration. **D** Representative BX-GAG fluorescence intensity images at 0, 1, and 2 h post-BX administration (scale bar 100 μm)

Compound 2

To the solution (10 ml) of dipyrromethane (1 mmol) in acetone, potassium carbonate (3 mmol) was added. The reaction mixture was stirred for 30 min at room temperature followed by the addition of propargyl bromide (3 mmol), which was stirred into the mixture overnight. The resulting crude material was dissolved in ethyl acetate, washed with water and saturated sodium chloride solution, dried over Na_2SO_4, and rotary evaporated under reduced pressure. The residue was purified by column chromatography yielding compound 2 (Fig. 1A (2)). ^{1}H NMR (CD_3Cl): δ 7.79 (s, 2H), 7.09 (d, J = 8.6 Hz, 2H), 6.88 (d, J = 8.6 Hz, 2H), 6.60 (s, 2H), 6.12 (dd, J = 2.73, 5.47 Hz, 2H), 5.86 (s, 2H), 5.33 (s, 1H), 4.62 (d, J = 2.34 Hz, 2H), 2.46 (t, J = 2.34 Hz, 1H).

Compound 3

Compound 2 (1 mmol) was dissolved in 10 ml of dry dichloromethane and tetrachloro-1,4-benzoquinone (1 mmol) was added. The reaction mixture was stirred at room temperature for 45 min. Et_3N (2 mmol) and BF_3OEt_2 (1 mmol) was subsequently added slowly and the reaction was stirred for an additional 2 h. The reaction mixture was diluted to 50 ml with dichloromethane, and then washed with water (50 ml) three times. The organic layer was dried over Na_2SO_4 and rotary evaporated under reduced pressure. The product was isolated by low-pressure flash silica column chromatography to yield the bodipy carrying triple bond (Fig. 1A (3)). ^{1}H NMR (CD_3Cl): δ 7.92 (s, 2H), 7.55 (d, J = 9.0 Hz, 2H), 7.13 (d, J = 8.6 Hz, 2H), 6.97 (d, J = 3.9 Hz, 2H), 6.55 (t, J = 1.2 Hz, 2H), 4.80 (d, J = 2.35 Hz, 2H), 2.61 (t, J = 2.34 Hz, 1H).

Compound 4

Deprotected xylosyl azide (1.2 mmol) was reacted with compound 3 (1 mmol) in the presence of sodium ascorbate (0.5 mmol) and Cu_2SO_4 (0.5 mmol) in acetone/water (1:1) mixture (20 ml). After the completion of the reaction, as confirmed by TLC analysis, the reaction mixture was concentrated using a rotary evaporator under reduced pressure. The reaction mixture was then purified using low-pressure flash silica column. ^{1}H NMR (CD_3OD): δ 8.31 (s, 1H), 7.91 (s, 2H), 7.54 (d, J = 8.2 Hz, 2H), 7.20 (d, J = 8.6 Hz, 2H), 6.98 (d, J = 3.5 Hz, 2H), 6.58 (s, 2H), 5.55 (d, J = 9.0 Hz, 1H), 5.29 (s, 2H), 4.00 (dd, J = 5.5, 11.3 Hz, 1H), 3.92 (t, J = 9.4 Hz, 1H), 3.72–3.54

(m, 1H), 3.51–3.45 (m, 2H); mass (ESI): calcd for $C_{23}H_{22}BF_2N_5O_5Na$ $[M + Na]^+$ 520.158, found 520.135. The final compound was purified by reverse phase C18 columns (compound 4; Fig. 1A (4)).

Animal Preparation

Methods followed those reported previously (Rabbitt et al., 2010). Briefly, adult oyster toadfish (*Opsanus tau)* of either sex, weighing ~500 g, with rostral-caudal length greater than 25 cm were obtained from the Marine Biological Laboratory in Woods Hole, MA. Each fish was anesthetized by immersion in tricaine methanesulfonate-treated seawater (50 mg/l, MS-222, Sigma), and the tail muscle was subsequently paralyzed by an intramuscular injection of pancuronium bromide and immobilized within a poly (methyl methacrylate) enclosure with aerated treated seawater submerging the gills and two thirds of the body. The eyes and remainder of the body were covered with moist kimwipes. A dorsal craniotomy was made to expose the horizontal canal ampulla, anterior canal ampulla, and utricular macula. Fluorinert (FC-770; 3 M) was injected in the dorsal section of the cranial cavity to improve optical access for fluorescence microscopy of vestibular organs in vivo. The anterior canal (AC) was cut proximal to the anterior ampulla for the delivery of BX, compound 4, and the cut ends were raised out of the surgical opening to prevent mixing of endolymph and perilymph. This preparation maintains normal sensitivity and background discharge of horizontal canal (HC) afferent neurons (Rabbitt et al., 2009; Rabbitt et al., 2010). The development of BX fluorescence in the crista ampullaris was monitored in vivo using an upright microscope (Zeiss, Axiotech, 493 nm/503 nm) fitted with a long working distance ×5 objective (Mitutoyo Plan Apo) and EMCCD camera (Qimaging, Rolera MX).

BX Treatment and Immunohistochemistry

On average, 10 nl of a 2-μM BX solution (in DMSO) administered via a pulled micropipette (1.2 mm borosilicate glass, pulled and cut) into the rostral limb of the cut anterior canal (Fig. 1B). To facilitate delivery, the micropipette was partially filled with endolymph from a donor fish, and ~ 10 nl BX solution was pulled into the tip of the same pipette. The rostral limb of the cut anterior canal was carefully lifted out of the surgical opening and exposed to air, and the pipette was lowered into the membranous lumen of the canal to inject the BX-endolymph solution. Administration disrupted the anterior canal cupula and generated a small flow of endolymph through the utricular (U) vestibule, up the common crus, and toward the caudal cut limb of the anterior canal. The function of the horizontal canal was not compromised, as evidenced by single unit afferent neural responses to mechanical indentation of the canal duct (Rabbitt et al., 1995). Either a BODIPY compound, BODIPY-FL (NHS ester; D6140, Invitrogen), unconjugated to xyloside (Compound 3), or FITC (Invitrogen) dyes were used as negative controls, administered using the same approach as BX. Unless otherwise noted, 4 h post BX or dye administration, the rostral section of the membranous labyrinth including the horizontal and anterior canal ampullae and utricular vestibule were dissected and harvested. In some cases, BX was also administered directly into the saccule via a fenestration of the saccular membrane. BX-treated saccules were treated in the living animal over the same time period as canals and harvested in a similar fashion. In some experiments, either FM1-43 (Invitrogen) or Neurobiotin 350 (~5 %; no. SP-115, Vector laboratories), was added directly to the anterior canal to label hair cells using the same approach described for BX administration. Once tissue was excised, samples were fixed (4 % paraformaldehyde, 0.25 % glutaraldehyde in PBS), for 1 h at RT or overnight at 4 °C, with the exception of tissue labeled using FM1-43 which was imaged fresh. Following fixation, tissues were either stained with phalloidin to visualize stereocilia (phalloidin-Alexa 568; A-12,380, Invitrogen) or stained for nuclei with DAPI (SlowFade; S36939, Invitrogen) as per the manufacturer's instructions. Alternatively, tissues were prepared for immunohistochemical experiments to examine endogenous proteins and GAGs using the following method. First, tissues were immersed in 1 ml blocking solution (5 % FBS, 1 % BSA, and 0.1 % PBS) for 1 h at room temperature. Second, tissues were immersed in blocking solution with the desired antibodies for immunohistochemical reactions. For endogenous chondroitin sulfate B recognition, a dilution of chondroitin sulfate mouse monoclonal antibody (1:100 dilution) was made (CS-56, Abcam) and tissues were incubated overnight at 4 °C. To check for the presence of heparin sulfate, a heparin sulfate rabbit polyclonal antibody was used (1:200 dilution) in PBS with 5 % FBS (HSPG, AbD Serotec), incubated overnight at 4 °C. In order to visualize kinocilia, an alpha-tubulin antibody was used (1:200 dilution PBS with 5 % FBS; (6-11B-1, Abcam)) and incubated with tissue overnight at 4 °C. Third, all tissues which were reacted with antibodies were subsequently washed three times (15 min each) in PBS, followed by incubating with species appropriate Alexa Fluor®

secondary antibody (Thermo Fisher Scientific), for 1 h at room temperature. Fourth, tissues were washed three times with PBS before being mounted for imaging on glass-bottom dishes (P35G-1.5-14-C, MatTek).

Characterization of GAGs from BX Treated Tissues

Intact BX-treated vestibular labyrinths were harvested for the characterization of GAG chains using two different approaches; visualization of GAGs was conducted ex vivo before or after treatment with heparin and/or chondroitin lyases. Briefly, tissues and cell membranes were permeabilized by submerging tissues in 0.1 % (*w/v*) Digitonin (dH_2O) for 30 min at 30 °C. Subsequently, the tissues were temporarily placed in glass-bottom dishes and immobilized by gently lowering a glass coverslip on top of the tissue in PBS. Initial imaging was performed using an upright confocal microscope (FV1000, Olympus) to acquire the baseline fluorescence of BX-GAGs, tissues were subsequently removed and placed in a microcentrifuge tube. The tissues were prepared for digestion of either chondroitin sulfate or heparin sulfates by the addition of the following buffers and corresponding enzymes; chondroitinase ABC buffer (50 mM Tris, pH 8.0, with 60 mM sodium acetate and 0.02 % bovine serum albumin) with chondroitinase ABC (chABC; C3667, Sigma) or heparinase digestion buffer (a 5× stock solution containing 1.25 M sodium acetate, 12.5 mM calcium acetate (pH 7, HCl)), diluted appropriately was used with heparinase I, II, and III enzymes (hepI, hepII, hepIII; H2519, H6512, H8891, Sigma). Enzymes were used at concentrations of 2.5 mU and incubated in enzyme buffer with samples at 37 °C for 16 h. Following incubation, the tissues were carefully washed with fresh PBS, mounted on clean glass-bottom dishes, and immobilized by the placement of glass coverslip on top of the tissue.

Cellular Physiology

In a subset of experiments, semicircular canal sensitivity to physiological stimulation was monitored before and after administration of BX, by recording semicircular canal microphonics and action potentials in single-unit afferent neurons. In brief, the micromechanical indentation of the slender membranous duct was applied to mimic physiological head rotation at angular frequencies from 1 to 5 Hz using methods reported previously (Rabbitt et al., 1995). Spontaneous afferent nerve discharge rate (spks s^{-1}) and sensitivity to mechanical indentation (spks s^{-1} μm^{-1}) were determined for each neuron. Modulation of the voltage in the endolymph relative to the perilymph (semicircular canal microphonic) was recorded using low impedance glass electrodes and lock-in amplification (Stanford Research SRS830) as reported previously (Rabbitt et al., 2005). The microphonic was monitored in the control condition and for 2–18 h after BX administration, to measure relative changes in whole-organ transduction current modulation in response to sinusoidal mechanical stimulation at 5 Hz (Rabbitt et al., 2005). The sensitivity of afferent discharge to heat pulses delivered to the semicircular canal hair cell epithelium by infrared (IR) light (spks s^{-1} $°C^{-1}$) was also recorded before and after BX administration to determine if BX treatment altered IR heat pulse responses (Rajguru et al., 2011; 400 µm fiber, 1862 nm, 200 µs, 50 pps, 60 % power, Lockheed Capella). Neurobiotin350 (NBN350; Vector Labs, Burlingame, CA) was introduced to the ganglion for retrograde bulk labeling of neuronal projections in the crista ampullaris. In other experiments, NBN350 was administered directly into the endolymph using the same approach described above for BX, following 2 h of incubation with BX, to serve as a proxy for MET function by monitoring the rapid uptake of NBN350 by hair cells. MET channels were blocked in control experiments with the known ototoxic aminoglycoside gentamicin (1 mM) to confirm that NBN350 uptake was via MET channels. The data presented are mean ± standard deviation unless otherwise noted.

Image Acquisition and Analysis

The material was imaged using either an Olympus FV1000 confocal microscope or a FV1200MPE multiphoton microscope with water immersion objectives (×40 or ×60). Additional postprocessing was conducted using FluoRender software.

Pharmacokinetic Model

We applied a six-degree-of-freedom pharmacokinetic model to interpret fluorescence as a function of time and location (Holman et al., 2015). The model lumps unbound BX and primed GAGs (BX-GAG) into three compartments, tracking six concentrations: BX in endolymph, BX in the cytoplasm, BX in the Golgi, BX-GAG in the Golgi, BX-GAG in the cytoplasm, and BX-GAG in glycocalyces. Production of xyloside-primed GAGs in the Golgi was assumed to follow the Michaelis-Menten kinetics. Mass balance provides the following set of differential equations for the number of

BX molecules (N_1, N_2, N_3), and xyloside primed GAGs (N_4, N_5, N_6) in each of the three compartments:

$$\frac{d\vec{N}}{dt} + M\vec{N} = \vec{F}; N_k \geq 0 \quad (1)$$

For a bolus delivery of BX into the extracellular media at time $t = 0^-$, the right-hand side is zero, $\vec{F} = \vec{0}$, and the initial concentration is $\vec{N}(0^+) = [N_0\ 0\ 0\ 0\ 0\ 0]^T$. The mass transfer matrix is sparse, with elements corresponding to inverse time constants between compartments and states. Although experiments were not sufficient to determine every parameter precisely, to aid in the interpretation of the results, we used $m_{11} = 0.08$, $m_{12} = -0.005$, $m_{16} = -0.5$, $m_{21} = -0.025$, $m_{22} = -25$, $m_{23} = -25$, $m_{32} = -25$, $m_{33} = 54$, $m_{43} = -4$, $m_{44} = 2.5$, $m_{54} = -2.5$, $m_{55} = 1.05$, $m_{56} = -0.05$, $m_{65} = -0.05$, and $m_{66} = 2.55\ s^{-1}$. The elements m_{33} and m_{43}evolved following the Michaelis-Menten kinetics approaching the values listed above at 36 h. Concentrations were determined by dividing by the BX accessible volume of each compartment $\Phi = [15\quad 8.10^{-6}\quad 1.6 \times 10^{-6}\quad 1.6{\cdot}10^{-6} 8.10^{-6} 6.10^{-7}]$ μL. Since this model lumps all extracellular glycocalyces together, it cannot address differences between GAG kinetics in various structures, such as the capillary glycocalyx vs. the kinociliary glycocalyx for example. To distinguish such spaces, additional degrees of freedom would be needed. Equation 1 was solved numerically in the time domain.

RESULTS

To examine glycosaminoglycan kinetics in vestibular organs, BX was introduced into the lumen of the anterior canal (AC) of the living animal using a glass pipette (p) and diffused passively into the utricular vestibule (U), AC ampulla, and horizontal canal (HC) ampulla (Fig. 1B, C). BX was rapidly taken up by hair cells and supporting cells, intensifying BX concentration within cells and generating a strong signal in the AC, U, and HC sensory epithelia. The time course of BX fluorescence signal intensity in the HC sensory epithelium was imaged at low magnification in vivo, revealing 50 % peak fluorescence after ~1 h and reaching peak overall intensity after ~2 h (Fig. 1C, normalized to 1 at the peak; n = 4). Signal was dominated by fluorescence in the sensory epithelium (Figs. 1D (1, c) and 2A). Fluorescence images were collected in vivo at random time intervals ~5–15 min apart without illuminating between image acquisitions. With a 15-min sampling interval in the horizontal canal crista, the time constant of fluorescence decay after the peak was ~23.8 h (also see Supplementary Movie 1). We confirmed that the reduction in BX signal was due to BX clearance (not photobleaching) by recording fluorescence in one animal at 1, 2, 3, and 13 h without the excitation illumination between images. The time constant of fluorescence decay in this case was ~23.0 h, nearly equal to the time constant found when imaging BX every 15 min. Results rule out photobleaching and confirm BX clearance was the dominant mechanism responsible for the reduction in whole-organ fluorescence over time (set primarily by rate constant k_e in Fig. 8).

To observe and verify delivery of BX into the canal, an unconjugated control xyloside (compound 3; see the "Methods" section) was coinjected with endogenous endolymph and fluorescein (FITC) into the lumen of the anterior canal. The xyloside with fluorescein did not produce any fluorescent signal in the sensory epithelium, and the weak, nonspecific fluorescence in the endolymph itself was cleared within 4 h (data not shown). We also tested a water-soluble BODIPY molecule (BODIPY-FL) as a control for the BODIPY, which appeared to fill the HC ampullary lumen; however, it was not incorporated into the hair cells, supporting cells, or vestibular ganglion (Fig. 2A; control). Similar to the FITC, 4 h postinjection, BODIPY-FL fluorescence was no longer observed in the endolymph. The contralateral ear of the fish treated with BODIPY-FL was administered BX, as described above, and a marked increase in signal developed over the same time period (4 h postinjection) in sensory epithelia (Fig. 2A, BX; scale bar: 50 μm). Unexpectedly, BX-GAGs were observed along what appeared to be afferent neurons (Fig. 2A (a)), in the cupula (Fig. 2A (c)), around kinocilia (Fig. 2A (s)), and in epithelial cells lining the membranous labyrinth. Based on these data, a more in-depth examination of BX-treated tissues was carried out, using 4 h post-BX administration as a benchmark time point.

We imaged cristae with a ×60 objective using the FV1000 confocal to resolve spatial distributions of BX-GAG. Two hours after BX administration, intense fluorescence was observed in the cytoplasm of hair cells and supporting cells (Fig. 2B; green: BX; blue: DAPI) and, at later times, developed in the cupula and areas surrounding the hair bundles. Bright field microscopic images were superimposed to better visualize the morphology of stereocilia (s) projecting into the cupula, hair cells (hc), and supporting cells (sc). Part of the BX signal was

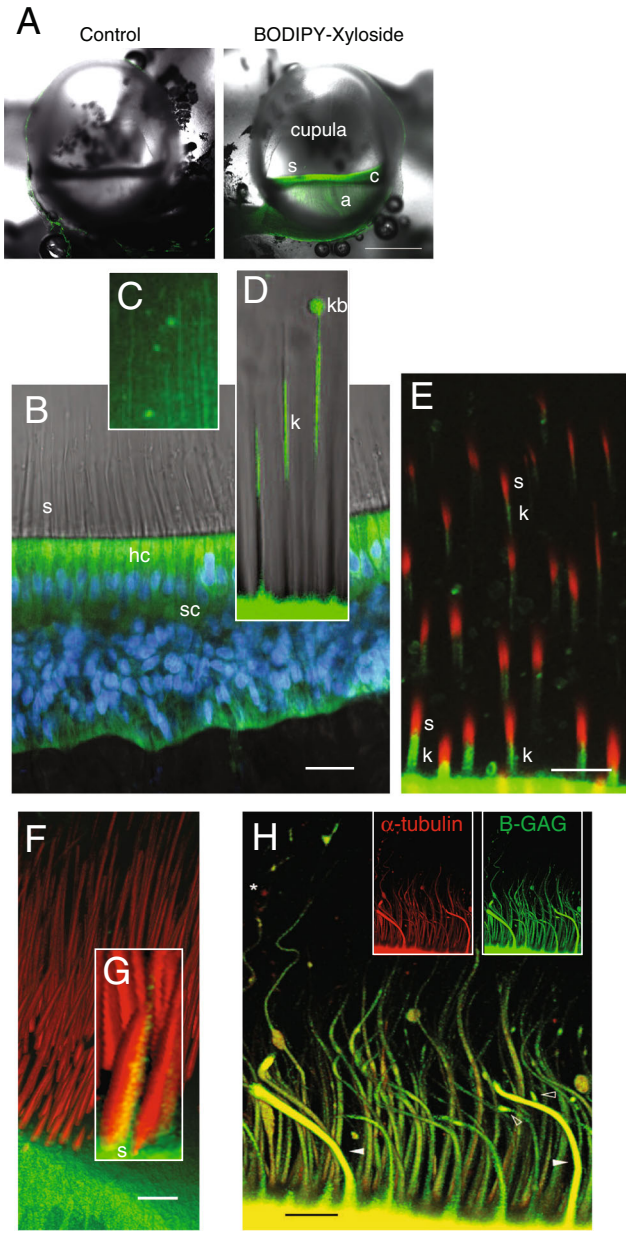

FIG. 2. In vivo properties of BX fluorescence in the crista ampullaris. **A** Bilateral confocal images of the left (control, BODIPY-FL alone) and right ampulla (BX) from the same animal, 5 h postadministration of each (scale bar 500 μm). BX-GAGs developed rapidly in hair cells and supporting cells within the sensory epithelium (*c*) but was slower to appear in the glycocalyx enveloping projections of afferent neurons in the crista (*a*). BX-GAGs also developed within the cupula and adjacent to stereocilia (*s*). **B** Within 15 min post-BX administration; BX-GAGs (*green*) were visible in hair cells (*hc*) and supporting cells; nuclei (DAPI, *blue*) were also visualized for cellular structure and orientation. Stereocilia (*s*) hair bundles are shown with transmitted light. **C** Weak lines of BX-GAG fluorescence running from the apical surface of hair cells to the apex of the ampulla developed within the cupula. **D** BX-GAGs appeared in a glycocalyx structure around kinocilia (*k*) and in some cases appeared to be terminated by a fluorescent bulb-like structure (*kb*) located ~80 μm above the apical surface of hair cells at the tip. Two-photon z-stack sections through hair bundles show stereocilia (phalloidin; *s, red*) adjacent to BX-GAGs enveloping kinocilium (*k; green*). The kinocilia (*k*) appears below stereocilia (*s*) due to the angle of the optical section through the hair bundles. **F** 3D rendering from the same z-stack as in **E** of hair cells and bundles projecting into the cupula. Inset **G**, BX-GAGs on the kinocilia side of the hair bundle (scale bars 50 μm). **H** Representative kinocilia (acetylated α-tubulin antibody, *red*), colocalized with BX-GAGs, in the crista ampullaris, following 4 h post-BX treatment in vivo. BX-GAGs appearing as glycocalyx (*white arrows*) surrounding kinocilia inside (*yellow*). Areas along kinocilia appear to have larger diameters due to handling of tissues and bending of the kinocilia that occurred (*arrows*). Some regions of kinocilia did not appear to have the BX-GAG glycocalyx (*star*; scale bar: 15 μm)

clearly extracellular and due to priming of BX-GAGs which were transported to the extracellular space. Increasing the excitation laser power revealed fluorescence in the striated bands in the cupula (BX-GAGs) running from the apex to the base (Fig. 2C). Based on molecular kinetics (see the "Discussion and model" section), the extracellular BX-GAGs would be expected to develop peak concentrations subsequent to the initial intracellular BX priming molecule. Four hours after BX treatment, BX-GAGs appeared in glycocalyces enveloping the hair cell kinocilia (Fig. 2D (k)), and terminating in what has been previously described as a kinociliary bulb (Fig. 2D (kb)). BX-GAGs (green) were observed around the kinocilium, adjacent to stereocilia (phalloidin-AlexaFluor 568; red) but did not appear to colocalize with stereocilia. An angled two-photon optical cross section through the semicircular canal hair bundles further demonstrates BX-GAGs adjacent to the stereocilia (Fig. 2E (s), and surrounding kinocilia (Fig. 2E (k)). Additional 3D reconstructions were generated from two-photon confocal z-stacks (Fig. 2F; Supplementary Movie 2), where the BX-GAGs were observed only on the kinociliary side of the hair bundles (Fig. 2G). In separate experiments, labeling with an acetylated α tubulin antibody following BX treatment confirmed BX-GAGs in a kinocilia glycocalyx extending along the length of kinocilia (Fig. 2H). One-micron thick sections through kinocilia (Fig. 2H, inset, red panel) acquired by confocal microscopy, suggests BX-GAGs colocalizing to the outside of kinocilia (Fig. 2H, merged yellow), although the specific location relative to the plasma membrane cannot be proven by this imaging technique. The curved shape and deflection of the kinocilia in this image is believed to have been due to ex vivo tissue postprocessing and whole mount handling. Solid arrowheads depict two representative kinocilia that, at some regions along the kinocilia, appeared to either lack BX-GAG glycocalyx or were obstructed from imaging (Fig. 2H, star).

Hair cells and supporting cells in the otolith organs developed BX and BX-GAGs over time. Two-photon imaging of the utricular macula revealed both intracellular and extracellular BX-GAGs (Fig. 3; phalloidin, red; BX-GAGs, green; DAPI, blue). Orthoganol projections helped to visualize BX-GAGs in extracellular striated patterns at the apical surface of the epithelium (Fig. 3A, inset). Closer examination of the BX-GAG lattice using a higher magnification objective (×60) revealed BX-GAGs projecting above the apical surface of the hair cells at junctions between the hair cells and the supporting cells (Fig. 3B). Images show the extracellular BX-GAG lattice aligning with the polarization of the hair cell bundles. Each kinocilium in the utricle was enveloped by a BX-GAG glycocalyx (Fig. 3B, arrow). Cross sections (Fig. 3C, D) show intracellular fluorescence in the hair cells and the supporting cells likely arising from concentrated BX (see model and Fig. 8), in addition to the extracellular BX-GAG lattice at the apical surface of the epithelium from a large z-stack throughout an intact utricle (3D).

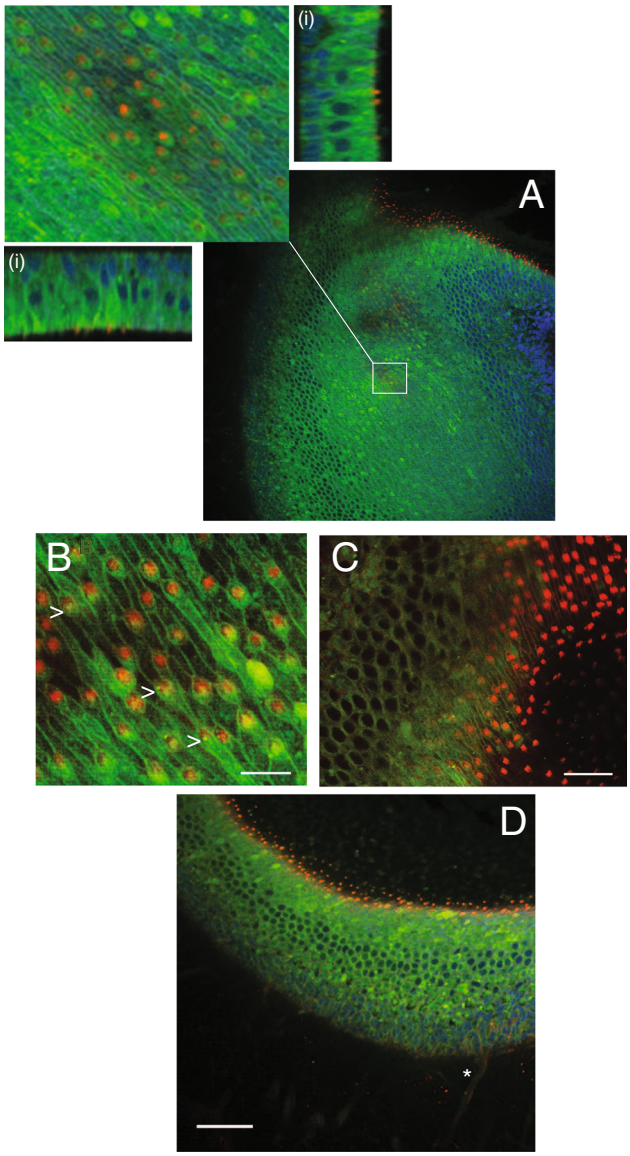

FIG. 3. Distribution of BX-primed GAGs in the utricle and saccule. Utricles were stained with DAPI (*blue*) and phalloidin (*red*) to visualize nuclei and stereocilia, respectively. **A** Two-photon projection of a z-stack image demonstrates the presence of BX-GAGs (*green*) in several structures in the utricular epithelium. Orthographic projections of an enlarged region of the utricular epithelium demonstrating the extent of BX-GAGs throughout utricular hair cells and supporting cells (*i*). **B** BX-GAGs at the apical face of hair cells formed a meshwork glycocalyx between cells that aligned with the local polarity of hair bundles. A fluorescent BX-GAG glycocalyx developed around each kinocilia (*arrows*; scale bar 10 μm). Stereocilia bundles (labeled *red*) project away from the cell bodies in the same orientation as the kinocilia resulting in the *yellow* appearance of *green* glycocalyx enveloped kinocilia (*arrow*). **C** Alternative lower magnification cross-sectional view of **B**, showing stereocilia bundles (*red*) projecting from the hair cells (*green*; scale bar 20 μm). **D** Cross-sectional view of the hair cells, supporting cells, kinocilia, and an afferent nerve (*star*) in a representative saccule (scale bar 50 μm)

BX-GAG incorporated into glycocalyces and appeared to envelop myelinated nerve fibers (Fig. 4A (a)), as they exited the basement membrane (bm). Initial heminodes (n) and afferent (a) fibers with BX-GAGs were observed at the floor of the basement membrane in multiple cristae (Fig. 4B; $n = 30$). Type I hair cells and calyx nerve terminals are not present in fish, and therefore, the results reported here are limited to afferents contacting type II hair cells with bouton terminals. Introduction of FM1-43 into the endolymph rapidly labeled the hair cells and the afferent nerve fibers (Fig. 4C, magenta; ~5 min post-FM1-43 introduction; scale bar 25 μm), rendering FM1-43 ineffective to test MET status in this preparation and suggesting potentially higher permeability of FM1-43 in fish relative to other preparations (Corey and Hudspeth, 1979; Meyers et al., 2003; Farris et al., 2004; Nishikawa, 1996; Gale et al., 2001; Meyers et al., 2003). This motivated the use of NB350 as an alternative molecular probe to test MET channel permeability as described below.

To examine the incorporation of BX-GAGs into afferent neuron membrane glycocalyces, the horizontal canal nerve was transected and the neurons were retrograde bulk labeled using Neurobiotin350 (NBN350). BX-GAGs appeared to be surrounding myelinated sections of afferent neurons (Fig. 4D, intracellular NBN350, blue; extracellular BX-GAG, green), forming a putative BX-GAG glycocalyx (g). Unmyelinated fibers (Fig. 4D, (inset u)) making bouton (b) contacts on hair cells appeared not to be enveloped by BX-GAG containing glycocalyces. BX-GAGs were also observed colocalizing with bouton endings at this level of resolution (Fig. 4D, (inset b)), suggesting the presence of BX-GAGs at the hair cell afferent synaptic terminals. The physiological role of GAGs at this synapse is not yet known.

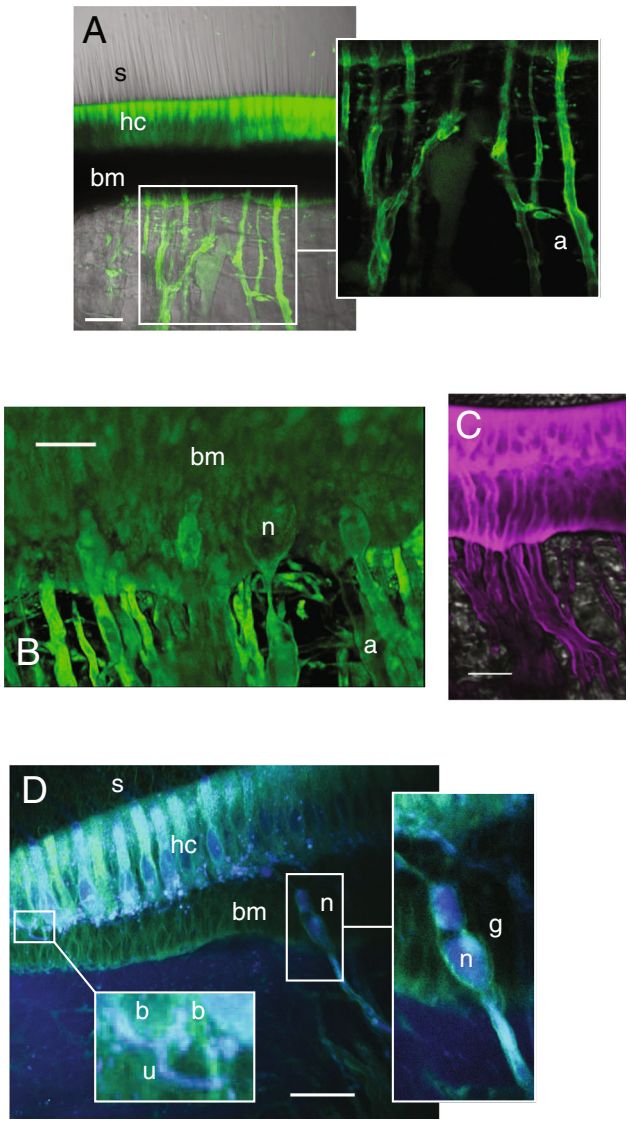

FIG. 4. Afferent nerve fibers and bouton terminals were partially enveloped by a BX-GAG glycocalyx (*green*). **A** BODIPY fluorescence was present in hair cell bodies (*hc*) and appearing to surround afferent (*a*) nerve fibers (scale bar 50 μm). **B** Higher magnification of BX-GAGs present in the basement membrane (*bm*) of crista and at heminodes (*n*) (scale bar 30 μm). **C** FM1-43 (*magenta*), injected into endolymph over the same time scale as that of BX (**B**), labeled hair cells and neurons; scale bar: 15 μm. **D** Maximum intensity of 20-μm two-photon projection following whole nerve intracellular labeling with NBN350 (*blue*) revealing colocalization of BX-GAGs (*green*) with bouton (*b*) nerve terminals. Unmylenated (*u*) dendrites branching to bouton terminals showed little evidence of BX-GAGs. The initial heminode (*n*) within the basement membrane (*bm*) of the crista ampullaris was enveloped by a xyloside primed glycocalyx (*g*) that continued to envelop the afferent (*a*) nerve fibers projecting centrally (scale bar 50 μm)

Since BX-GAGs were present in the kinociliary glycocalyx and to a lesser extent in the cupula, we hypothesized that MET might be altered by BX administration. We tested the function of MET channels following BX administration by recording semicircular canal microphonics in response to sinusoidal stimuli and by examining entry of NBN350 into hair cells. Although NBN350 is quite large (573 g mol^{-1}), robust NBN350 labeling in the cytoplasm of utricular hair cells was observed when introduced into the endolymph of the toadfish (Fig. 5A; scale bar: 15 μm). However, NBN350 did not enter the hair cells and was restricted to extracellular space when MET was blocked with the known ototoxic aminoglycoside gentamicin (1 mM) (Fig. 5B). To be consistent with the other BX experiments in this report, we introduced NBN350 2 h after administration of BX, to allow for priming of new BX-GAGs prior to testing MET channel permeability to NBN350. Figure 5C, D shows that following BX administration, only a subset of hair cell soma exhibited NBN350 (blue) in this condition; thus, indicating that not all MET channels were permeable to NBN350 ($n = 4$). In the crista (Fig. 5C), a subset of hair cells showed NBN350 in hair bundles (inset) and soma (Fig. 5C (1)), while others did not (Fig. 5C (2)). Differential uptake of NBN350 was more obvious in plan view sections of the utricular macula where all cells showed the presence of BX-GAGs (Fig. 5D–F), but only a subset showed NBN350 (Fig. 5D, E; blue). The results are summarized in Fig. 5G (blue, cross hatched) for hair cells in the utricular macula as the fraction of MET channels permeable to NBN350, indicating that only 24 % of hair cells had functional MET channels 2 h post-BX administration.

To further explore MET function, we recorded semicircular canal microphonics during sinusoidal mechanical indentation of the horizontal canal (Rabbitt et al., 2005). On average, the microphonic was reduced to 20 % of its magnitude in the control condition 2 h post-BX administration (gray bar), indicating that modulation of the net MET current was reduced substantially after introduction of BX. The magnitude of microphonic reduction was consistent with the number of hair cells that were no longer permeable to NBN350. There was a partial recovery of the microphonic 18 h post-BX administration, where the microphonic was 53 % of the control level. The time course of microphonic recovery was consistent with the time course of clearance of BX and BX-GAGs providing further evidence that interference with MET was due to action of the compound and not due to an unknown secondary effect (also see the "Discussion of model" section; Fig. 8).

To examine the physiological consequences of BX administration on action potentials in semicircular canal afferent neurons, we recorded background discharge rate (spk s^{-1}), sensitivity to mechanical stimulation (spk s^{-1} μm^{-1}), and sensitivity to infrared heat pulse stimuli (spk s^{-1} C^{-1}). Population averages

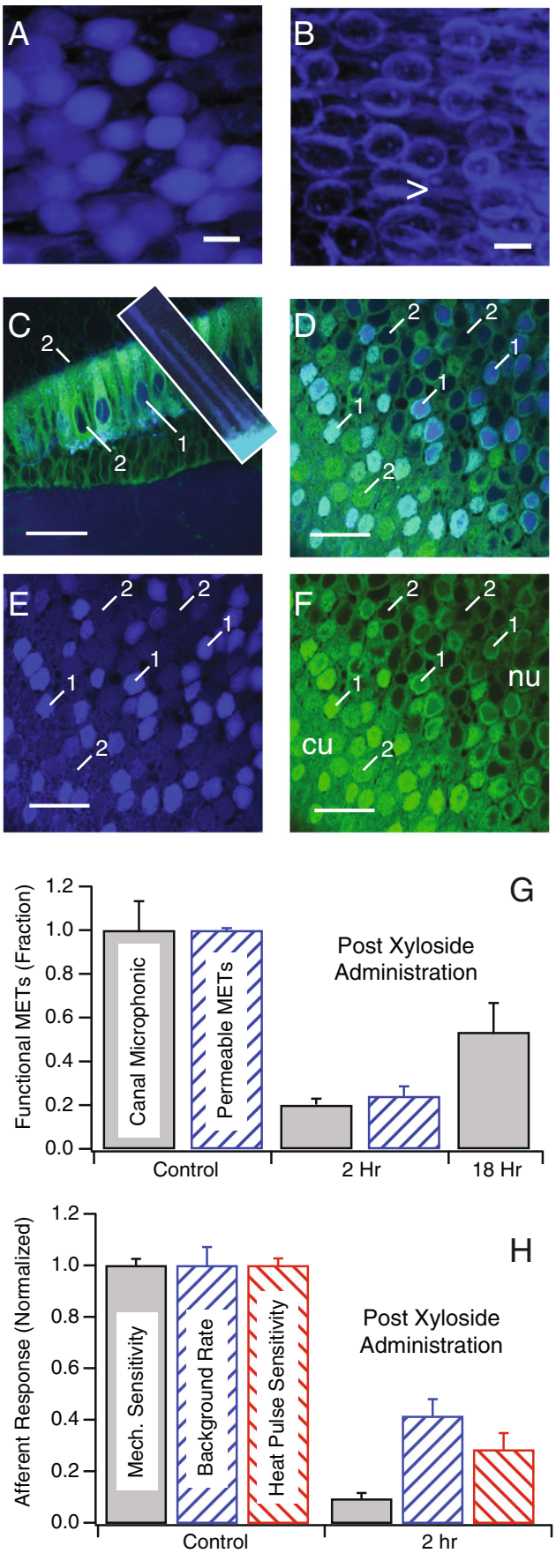

FIG. 5. Hair cells from saccule-staining positive for NBN350 (*blue*) following administration into the endolymph of the living oyster toadfish for 2 h, either without gentamicin (**A**) or with 1 h pretreatment of gentamicin (1 mM) (**B**). **C–F** Two-photon images of functional (*1*) vs. blocked METs (*2*) in the semicircular canal crista (**C**) and in the utricular macula (**D–F**). NBN350 (*blue*) labeled cilia of hair bundles (**C**, inset). **G** Semicircular canal microphonics recorded in response to mechanical stimulation show MET currents were reduced to 20 % 2 h after BX administration and recovered to 53 % 18 h after administration (n = 5). The *inset* shows reduction of the microphonic in three example animals (onset time constant ~25 min). Twenty-four percent of hair cells in the utricular macula labeled for functional METs 2 h after BX administration, confirming that ~75 % of hair cell MET channels were blocked by the BX compound (n = 5). **H** Single-unit afferent discharge rates were reduced (n = 47) following BX treatment. The average afferent discharge rate (spk s^{-1}) decreased 59 %. **H** Sensitivity to sinusoidal mechanical stimulation at 5 Hz (spks s^{-1} μm^{-1}) decreased 91 % re: controls, while sensitivity to infrared heat pulse stimulation (spks s^{-1} $°C^{-1}$) of the crista ampullaris decreased 71 % re: controls. *Error bars* show standard error of the mean (**A**, **F**), with all results normalized to the animal-specific mean in the control condition prior to BX administration (scale bars: 15 µm, Fig. 5**A–B**; 50 µm, Fig. 5**C–F**)

recorded prior to BX administration were used as controls to normalize results. The background discharge rate (spk s^{-1}) decreased 59 % compared with the controls, 2 h post-BX treatment (Fig. 5H). This may be due, in part, to the reduction in MET currents, which would be expected to lead to the hyperpolarization of hair cells and a reduction in tonic transmitter release. This was less than the reduction in MET function, most likely because some vestibular afferent neurons exhibit spontaneous discharge even in the absence of input from hair cells. The reduction in sensitivity to 5 Hz sinusoidal stimulation (spk s^{-1} μm^{-1}) was dramatic at 91 % re: controls (Fig. 5H, gray bars). This was larger than the reduction in microphonic, but the difference could partially reflect a sampling bias present in single-unit recordings that was absent in whole-organ microphonics. We also tested sensitivity of the same afferents to IR heat pulses (spk s^{-1} C^{-1}) applied to the crista. It has been argued previously that IR heat pulses directly evoke synaptic vesicle release in addition to modulating ion channel conductance and capacitive depolarization (Rajguru et al., 2011; Liu et al., 2014; Rabbitt et al., 2016). Therefore, the expected changes in sensitivity to IR heat pulses after BX administration would be less than the changes in sensitivity to mechanical stimulation. This was partially true, in that BX administration reduced sensitivity to IR heat pulses by 71 % relative to 91 % for mechanical stimuli in the same afferents (Fig. 5H, red vs. gray bars). A 71 % reduction, however, is still quite large and

implies that BX partially reduced heat pulse-evoked transmitter release from hair cells. At least part of this reduction was due to the blocking effect of BX on MET currents, which would cause the hair cells to become hyperpolarized and reduce heat pulse-evoked synaptic vesicle release. But, the present data cannot exclude an additional direct effect caused by changes in GAGs at the synapse.

We observed that synthesis of BX-GAGs from BX was time dependent, with kinetics varying between different cell types and extracellular structures in vivo. This heterogeneity caused the spatial distribution of BODIPY signals to vary over time, complicating studies of endogenous GAGs and BX-GAGs. With this caveat in mind, using a monoclonal chondroitin sulfate antibody (CS-56), immunohistochemistry (IHC) revealed partial colocalization with BX-GAGs and chondroitin sulfate B (CSB) (Fig. 6A; middle panel, yellow). CSB appeared to transverse isotropic spindles extending in parallel from the crista toward the apex of the ampula (Fig. 6A, red), whereas the BX-GAGs appeared as larger vertical structures, supporting further evidence of a BX-GAG kinocilia glycocalyx, in addition to bulb-like structures at the tips of kinocilia (Fig. 6A, green). Hair cells and supporting cells in the crista also revealed the presence of CSB GAGs in discrete puncta (Fig. 6B, red); however, there appeared to be minimal colocalization of CSB and BX-GAGs, which was more diffuse. The basement membrane and glycocalyx around myelinated nerves appeared to have BX-GAGs, but the level and distribution of CSB was markedly different (Fig. 6C). Similar experiments were performed in the utricle, and results recapitulated the different signals of BX-GAGs colocalizing albeit minimally with punctate CSB in sensory epithelia and nerve glycocalyces (Fig. 6D, yellow).

Several additional methods in addition to IHC were tested to discern the types of GAGs being primed by BX. Using differential digestions with an array of lyases provided reproducible evidence that chondroitin sulfate B was the leading GAG primed by BX in this model system. Vestibular organs were harvested 4 h after BX administration and imaged prior to different lyase treatments (Fig. 7A). Tissues from semicircular canals were placed in a permeabilization buffer containing digitonin followed by incubating with either chondroitinase A, B, or C (data not shown) or a combination of all, chABC (Fig. 7B, C). The extent of digestion was found by taking regions of the images before (Fig. 7C (1)) and after digestion (Fig. 7C (2)), registering the images in software (IgorPro, WaveMetrics), normalizing fluorescence intensities, and subtracting the difference. The subtracted image (Fig. 7C) shows

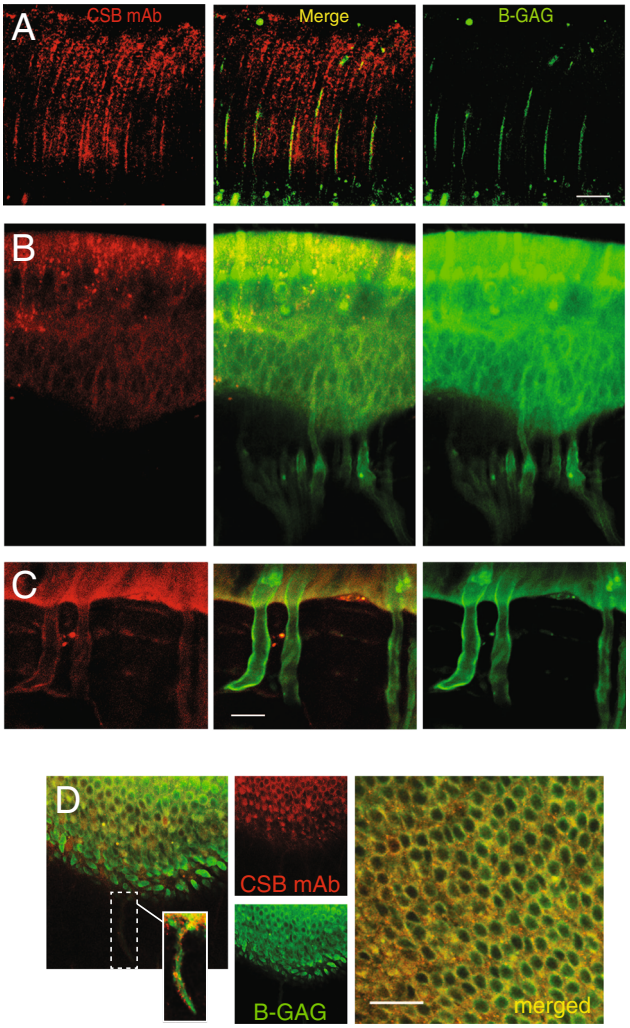

FIG. 6. **A** Chondroitin sulfate B antibody (CSB, *red*) revealed the anisotropic structure of the cupula surrounding hair bundles. BX-GAGs (*green*) colocalized with some CSB in the kinociliary glycocalyx, at the 4-h fixation time point, but not with CSB structures between kinocilium (merge panel, *yellow*). **B** Chondroitin sulfate B and BX-GAGs colocalized around hair cell bodies and less in supporting cells (*yellow*), with CSB yielding punctate fluorescence in HCs specifically. **C** In neurons, BX-GAGs were localized around the plasma membrane, while the presence of CSB had a weaker signal, it also colocalized with the membrane. **D** Colocalization of CSB and BX-GAG fluorescence was observed around cell bodies and afferents in the utricular sensory epithelium

that BX-GAGs were concentrated in the glycocalyces (g), around nerve fibers (n), and on the floor of the basement membrane (bm). The priming of BX-GAGs and their distribution in hair cells of the utricle (Fig. 7D) were also examined in an effort to determine GAG specificity from BX in different cell types from different tissues in vivo. Whole utricles were carefully dissected following treatment and cells were permeabilized and digested as described above for other vestibular organs with either chABC (Fig. 7D, (i)) or hepI, hepII, hepIII (Fig. 7D, (ii)).

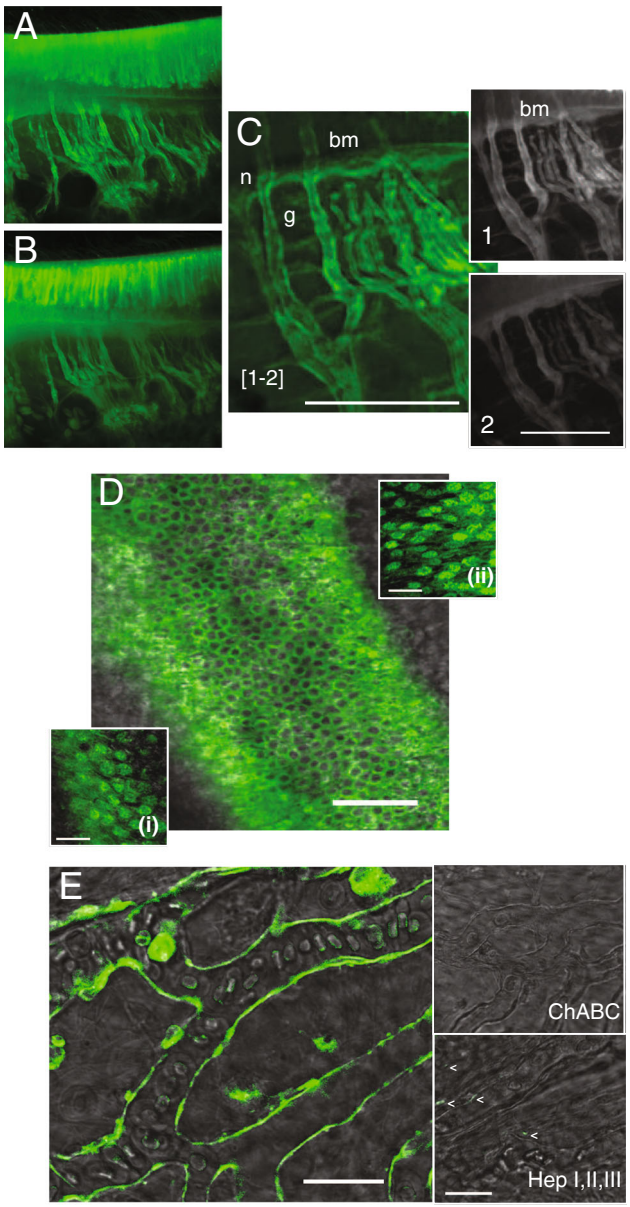

FIG. 7. ChABC digested extracellular BX-GAGs in glycocalyces. **A** BX-GAGs visualized in different cells and regions of the crista ampullaris before chABC digestion. **B** Remaining BX-GAGs following chABC. **C** Magnified region of tissue demonstrating final signal of BX-GAGs by subtracting fluorescence postdigestion (*2*), from predigestion (*1*). **D** Qualitative fluorescence levels of BX-GAGs in hair cells of the utricle were not effected by either chABC (*i*) or hepI, hepII, hepIII (*ii*). E, Capillaries supplying the saccular macula developed BX-GAG fluorescence in the glycocalyx and was eliminated following 18-h digestion with chABC. HepI, hepII, hepIII partially reduced BX-GAG signal in the capillary glycocalyx

BX-GAG fluorescence appeared to remain consistent to levels observed in other cell types. However, the BX-GAG glycocalyx appearing as an envelope around capillaries of the utricle was completely digested by chABC and not fully digested by hepI, hepII, hepIII (Fig. 7E).

Results demonstrate that the fluorescence signals observed in this study reflect a dynamic mix of molecular states including BX and BX-GAGs, of which a subset of BX-GAGs were digested with lyases. To describe the kinetics and distribution of BX and BX-GAGs, we developed a six-degree-of-freedom pharmacokinetic model of uptake and priming in hair cells (Fig. 8A). In the model, when BX is delivered to the endolymph (Fig. 8A (C_1)), it is rapidly taken up by cells (Fig. 8A (C_2)) and transported via the cytoplasm (Fig. 8A (C_2)) to the Golgi apparatus (Fig. 8A (C_3)). BX appeared to increase in fluorescence intensity during this process as the BX compound itself becomes concentrated in the cells. Once in the Golgi, BX-GAGs are synthesized (Fig. 8A (C_4)), and subsequently move through the cytoplasm (8 A; C_5) to extracellular glycocalyces (Fig. 8A (C_6)). Extracellular fluorescence of BX in the endolymph is weak because of the relative large fluid volume (Fig. 8B (C_1)). Over time, extracellular fluorescence becomes dominated by BX-GAGs concentrated in glycocalyces (Fig. 8B (C_6)), where the intensity is much higher than the original BX fluorescence in endolymph because of the localized concentration. This prediction is consistent with experimental data where BX-GAGs were observed after 4+ h in the kinociliary glycocalyx (Fig. 2D–H), in the cupula (Fig. 2C), above apical tight junctions between utricular and saccular hair cells (Fig. 3B), in afferent nerve fiber glycocalyces (Fig. 4), and in the capillary glycocalyces (Fig. 7E). Also consistent with experimental data, the model predicts significant intracellular signals primarily arising from the BX compound prior to GAG priming, followed by the development of punctate BX-GAGs in Golgi. The intensity of the intracellular BX in hair cells is predicted to exceed BX-GAGs in extracellular glycocalyces, consistent with experimental observations (e.g., Figure 2B vs. Figure 2D, E, excitation and detection gain were increased to observe BX-GAGs in the kinociliary glycocalyx relative to cell bodies).

DISCUSSION

In the present study, we describe the synthesis of a novel fluorescent xyloside (BX) and its properties when administered into the semicircular canal of oyster toadfish in vivo. The BX compound passively crossed cell membranes, appearing concentrated in sensory epithelia and rapidly initiated priming of BX-GAGs. Epifluorescence and confocal and two-photon microscopy techniques were used to detect

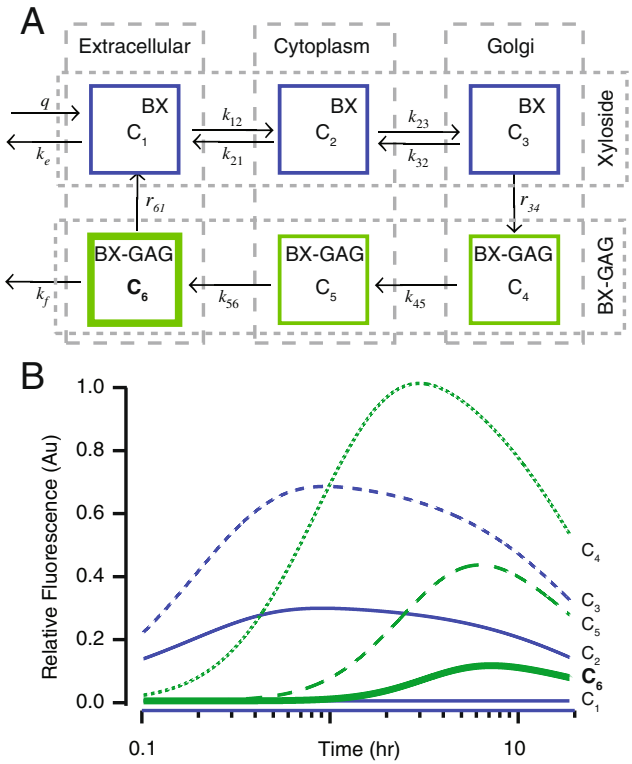

Fig. 8. **A** Six-degree-of-freedom pharmacokinetic model including (C_1) xyloside (*BX*) delivery into the extracellular space, (C_2) reversible BX entry into the cytoplasm, (C_3) reversible BX entry into the Golgi, (C_4) Michaelis-Menten kinetics to produce BX-GAG in the Golgi with BX core, (C_5) BX-GAGs exit the Golgi, (C_6) BX-GAG exits the cell and localizes in the extracellular glycocalyx, and (C_6) BX and BX-GAGs is cleared from the extracellular space through metabolism. **B** Simulated concentrations of either BX or BX-GAGs as functions of time. In silico, BX was rapidly taken up by the cytoplasm (C_2 + C_3) and Golgi (C_4), ultimately priming BX-GAG (C_5). BX-GAGs migrated to extracellular glycocalyces (C_6), reaching a plateau 5–7 h after the initial bolus injection

BX and BX-GAG distribution in the vestibular semicircular canals and otolith organs over time. Interpretation of imaging must take into account the original BX as well as primed GAGs (BX-GAGs), which are not distinguishable by these imaging techniques alone. To address GAG priming, differential enzymatic chondroitinase ABC or hepI, hepII, and hepIII digestions were conducted. The detection of membrane-associated signals (putative extracellular BX-GAGs) was significantly diminished following chondroitinase ABC treatment; however, intracellular fluorescence signals were not completely eliminated after cellular permeabilization and digestion. We postulate that either BX was immobilized intracellularly through GAG-independent interactions or intracellular BX-GAGs were inaccessible to enzymes within this system. Specific BX-GAGs would be expected to dissipate following lyase treatment, while GAG-independent BX may persist. To assist in the interpretation of data, we used a six-compartment pharmacokinetic model where fluorescence arises from GAG-independent BX and BX-GAGs. Simulations demonstrate that the BX signal is expected to follow differing time courses in the following compartments: Golgi, cytoplasm, and extracellular glycocalyces. BODIPY signal in each compartment was assumed to be proportional to BX and BX-GAG concentrations, and hence, reflects the compartment volume as well as accumulation of BODIPY molecules within the compartment. Focusing attention on the development of the signals from BX-GAGs within specific compartments therefore simplifies interpretation.

The presence of a negatively charged stereociliary glycocalyx in the auditory system of mammals has been previously reported (LeBoeuf et al., 2011). In canals of the vestibular system, we observed a tubular BX-GAG containing glycocalyx around the kinocilium and projecting into the cupula. The putative BX-GAG glycocalyx was terminated by a bulb-like structure located at the apical tip of the kinocilium. In the otolith organs, the kinociliary glycocalyx with BX-GAGs projected into the otolithic membrane. It has been suggested that GAGs may constitute up to one fifth of the molecules within the cupula (Tauber et al., 2001), but their specific physiological and biochemical constituents have not been fully documented to date. Present data from lyase treatments suggest that BX facilitates priming of chondroitin sulfate B; however, since GAGs are not template driven and lack proofreading capabilities, heterogeneity and structural diversity is expected, specifically with respect to sulfation patterns among GAG populations.

Through direct and indirect immunofluorescence microscopy techniques, we observed a kinociliary glycocalyx, composed of BX-GAGs. This glycocalyx may contribute a structural component for coupling hair bundles to accessory structures and may also contribute to normal vestibular mechanosensation. Incorporation of BX-GAGs, into what we describe as a kinociliary glycocalyx, was rapid and developed within 4 h along the entire 80+-μm length of the kinocilium in the semicircular canals. This high turnover may reflect the importance of a kinociliary glycocalyx to sensory transduction in vestibular organs. Additionally, BX-GAGs were observed within the translucent area above the hair cells, which has previously been described as thsubcupular space (Dohlman 1971), This lend further evidence that this space is not void but rather contains structural and potentially physiologically important functional carbohydrate-rich connective material (Santi and Anderson, 1986; Silver et al., 1998).

Incorporation of BX-GAGs into the cupula was considerably slower than the kinociliary glycocalyx, with relatively weak BX-GAG signals developing near the apex of the ampulla after 6 h. The time required to detect BX-GAGs at the apex of the cupula was consistent with the time required for damaged cupulae to reattach at the apex following modest mechanical insult (Rabbitt et al. 2009). Present data suggest that GAGs generated in the sensory epithelium are involved in dynamic maintenance of the cupula and self-assemble within the cupula as they move from the apical surface of hair cells to the apex of the ampulla. Complete cupula regeneration and self-assembly can occur, at least in fish (Rabbitt et al. 2009), but mechanisms remain largely unknown. It is remarkable that this highly organized molecular self-assembly occurs over a distance exceeding 500 μm in the acellular K^+-rich endolymph.

MET channel permeability was reversibly blocked following BX administration, as shown by a reduction in the semicircular canal microphonic to physiological stimulation and by reduced uptake of NBN350 from endolymph by hair cells. Exogenous xyloside treatments, which prime free GAG chains, have been shown by others to interfere with endogenous GAG synthesis through competitive inhibition, with the potential for disrupting physiological activities in several organs including the kidney (Platt et al. 1987), heart (Peal et al. 2009), and epithelial cells in vitro (Rapraeger 1989). Preliminary findings suggest BX preferentially primes chondroitin sulfates, potentially at the expense of endogenous GAG production and loss of function. If true, this could underlie the negative effect of BX on semicircular canal sensitivity to physiological stimuli. Based on our pharmacokinetic model (Fig. 8), BX fluorescence would be expected to develop in hair cells (Fig. 8B (C_2-C_5)) well before priming of extracellular BX-GAGs (Fig. 8B (C_6)), with extracellular BX-GAGs just beginning to appear 90 min after introduction of BX into the endolymph. The time course of the reduction in MET channel permeability observed experimentally (Fig. 5G, inset) was slower than would be expected if the initial blockage was due to direct action of BX (Fig. 8B (C_1 and C_2)) but faster than would be expected if the blockage was due to primed BX-GAGs in the extracellular matrix (Fig. 8B (C_6)). Although these theoretical considerations do not rule out other possibilities, the timing favors the hypothesis that MET permeability might have been blocked or disrupted by the appearance of BX-GAGs or competitive loss of endogenous GAGs (Fig. 8B (C_5)) at the site of the transducer itself. This model hypothesis is also consistent with recovery of the microphonic observed at longer time points (compare Figs. 5G vs. 8B (C_5)).

There is growing evidence of the importance and multiple roles for GAGs and glycoproteins in the development, homeostasis, and disease of the inner ear (Go et al. 2011). Two auditory and vestibular glycoproteins, OTOG and OTOGL, respectively, are among acellular components of the inner ear tectorial membrane and cupula (Cohen-Salmon et al. 1997; Yariz et al. 2012). A knockout was generated to the corresponding OTOG gene, otogelin, and these mice had effected cupula which were detached from the crista (Simmler et al., 2000). Further genetic mutations of otogelin, such as the autosomal recessive non-syndromic deafness-18B (DFNB18B), have been shown to be responsible for causing deafness and imbalance in mice (El-Amraoui et al. 2001; Schraders et al. 2012). At the amino acid level, OTOG contains 17 putative N-glycosylation sites, none of which have been identified for their carbohydrate specificity thus far. Future development of biochemical techniques for detecting such small quantities of GAGs, in conjunction with new molecular and optical tools such as BX, could further launch a better understanding into the complex roles of GAGs in the inner ear.

ACKNOWLEDGMENTS

The authors would like to thank Drs. Meghan Thompson and Umesh R. Desai at Virginia Commonwealth University for the capillary electrophoresis method development and data analysis. Also, Kelsey Kachnik, Rhiannon Johnson, and Nolan Ostberg are acknowledged for helping maintain the toadfish and cell lines, as well as Dr. Chris Rodesch at the University of Utah's Fluorescence Microscopy Core Facility, who gave valuable microscopy assistance. This work was made possible through the funding by the National Institutes of Health: Fluorender: An Imaging Tool for Visualization and Analysis of Confocal Data, National Institute of General Medical Sciences (Grants GM098151-01 and GM103545-17); the National Institute on Deafness and Other Communicative Disorders (Grant DC006685 to R.D.R.); and the National Heart, Lung, and Blood Institute (Grant HL107152 to B.K.).

Author Contributions H.A.H. performed in vitro and in vivo experiments, imaging and analysis, and conceived and wrote the manuscript. V.M.T. and B.K. conceived and synthesized the BX compound. S.A. synthesized a control xyloside compound. B.K. and R.D.R. conceived using BX in the oyster toadfish vestibular system. B.K. and R.D.R. supervised the project. L.N.N. and R.D.R. conducted electrophysiological experiments. M.K. contributed by providing glycobiology expertise.

COMPLIANCE WITH ETHICAL STANDARDS

Ethical Approval All animal procedures were approved by the University of Utah Institutional Animal Care and Use Committee and were conducted strictly in accordance with the relevant protocol.

Conflicts of Interest The authors declare that they have no conflicts of interest.

REFERENCES

Albiñana E, Gutierrez-Luengo J, Hernández-Juarez N, Baraibar AM, Montell E, Vergés J, García AG, Hernández-Guijo JM (2015) Chondroitin sulfate induces depression of synaptic transmission and modulation of neuronal plasticity in rat hippocampal slices. Neural Plast. doi:10.1155/2015/463854

Chicoine LM, Suppiramaniam V, Vaithianathan T, Gianutsos G, Bahr BA (2004) Sulfate- and size-dependent polysaccharide modulation of AMPA receptor properties. J Neurosci Res 75(3):408–416

Cohen-Salmon M, El-Amraoui A, Leibovici M, Petit C (1997) Otogelin: a glycoprotein specific to the acellular membranes of the inner ear. Proc Natl Acad Sci U S A 94:14450–14455

Corey DP, Hudspeth AJ (1979) Ionic basis of the receptor potential in a vertebrate hair cell. Nature 281:675–677

Dohlman GF (1971) The attachment of the cupulae, otolith and tectorial membranes to the sensory cell areas. Acta Otolaryn:89–105

El-Amraoui A, Cohen-Salmon M, Petit C, Simmler MC (2001) Spatiotemporal expression of otogelin in the developing and adult mouse inner ear. Hear Res 158:151–159

Farris HE, LeBlanc CL, Goswami J, Ricci AJ (2004) Probing the pore of the auditory hair cell mechanotransducer channel in turtle. J Physiol 558:769–792

Frischknecht R, Heine M, Perrais D, Seidenbecher CI, Choquet D, Gundelfinger ED (2009) Brain extracellular matrix affects AMPA receptor lateral mobility and short-term synaptic plasticity. Nat Neurosci 12(7):897–904

Gale JE, Marcotti W, Kennedy HJ, Kros CJ, Richardson GP (2001) FM1-43 dye behaves as a permeant blocker of the hair-cell mechanotransducer channel. J Neurosci 21:7013–7025

Gil-Loyzaga P, Raymond J, Gabrion J (1985) Carbohydrates detected by lectins in the vestibular organ. Hear Res 18:269–272

Go S, Yoshikawa M, Inokuchi J-I (2011) Glycoconjugates in the mammalian auditory system. J Neurochem 116:756–763

Holman HA, Tran VM, Nguyen LY, Arungundram S, Kalita M, Kuberan B, Rabbitt RD (2015) Xyloside primed glycosaminoglycans alter hair bundle micromechanical coupling and synaptic transmission: pharmacokinetics. 1703:030016.

Huang ML, Godula K (2014) Priming the cellular glycocalyx for neural development. ACS Chem Neurosci 5:873–875

Hultcrantz M, Bagger-Sjoback DAN (1996) Inner ear content of glycosaminoglycans as shown by monoclonal antibodies. Acta Otolaryngol 116:25–32

Katori Y, Hackney CM, Furness DN (1996) Immunoreactivity of sensory hair bundles of the guinea-pig cochlea to antibodies against elastin and keratan sulphate. Cell Tissue Res 284:473–479

Kleene R, Schachner M (2004) Glycans and neural cell interactions. Nat Rev Neurosci 5:195–208

Kochlamazashvili G, Henneberger C, Bukalo O, et al. (2010) The extracellular matrix molecule hyaluronic acid regulates hippocampal synaptic plasticity by modulating postsynaptic L-type Ca2+ channels. Neuron 67(1):116–128

Kuberan B, Ethirajan M, Victor XV, Tran V, Nguyen K, Do A (2008) Click" xylosides initiate glycosaminoglycan biosynthesis in a mammalian cell line. Chem BioChem 9:198–200

LeBoeuf AC, Ó Maoiléidigh D, Hudspeth AJ (2011) Divalent counterions tether membrane-bound carbohydrates to promote the cohesion of auditory hair bundles. Biophys J 101:1316–1325

Liu Q, Frerck MJ, Holman HA, Jorgensen EM, Rabbitt RD (2014) Exciting cell membranes with a blustering heat shock. Biophys J 106:1570–1577

Matani P, Sharrow M, Tiemeyer M (2007) Ligand, modulatory, and co-receptor functions of neural glycans. Frontiers in bioscience: a journal and virtual library 12:3852–3879

Meyers JR, MacDonald RB, Duggan A, Lenzi D, Standaert DG, Corwin JT, Corey DP (2003) Lighting up the senses: FM1-43 loading of sensory cells through nonselective ion channels. J Neurosci 23:4054–4065

Nguyen TKN, Tran VM, Sorna V, Eriksson I, Kojima A, Koketsu M, Loganathan D, Kjellén L, Dorsky RI, Chien C-B, Kuberan B (2013) Dimerized glycosaminoglycan chains increase FGF signaling during zebrafish development. ACS Chem Biol 8:939–948

Nishikawa (1996) < J Histochem cytochem-1996-Nishikawa-733-41.pdf > .

Okayama M, Kimata K, Suzuki S (1973) The influence of p-nitrophenyl beta-d-xyloside on the synthesis of proteochondroitin sulfate by slices of embryonic chick cartilage. J Biochem 74:1069–1073

Peal DS, Burns CG, Macrae CA, Milan D (2009) Chondroitin sulfate expression is required for cardiac atrioventricular canal formation. Developmental dynamics: an official publication of the American Association of Anatomists 238:3103–3110

Platt JL, Brown DM, Granlund K, Oegema TR, Klein DJ (1987) Proteoglycan metabolism associated with mouse metanephric development: morphologic and biochemical effects of beta-D-xyloside. Dev Biol 123:293–306

RABBITT RD, BOYLE R, HOLSTEIN GR, HIGHSTEIN SM (2005) HAIR-CELL VERSUS AFFERENT ADAPTATION IN THE SEMICIRCULAR CANALS. J NEUROPHYSIOL 93:424–436

RABBITT RD, BOYLE R, HIGHSTEIN SM (1995) Mechanical indentation of the vestibular labyrinth and its relationship to head rotation in the toadfish, *Opsanus tau*. J Neurophysiol 73:2237–2260RABBITT RD, BRENEMAN KD, KING C, YAMAUCHI AM, BOYLE R, HIGHSTEIN SM (2009) Dynamic displacement of normal and detached semicircular canal cupula. J Assoc Res Otolaryngol 10:497–509

RABBITT RD, BOYLE R, HIGHSTEIN SM (2010) Mechanical amplification by hair cells in the semicircular canals. Proc Natl Acad Sci 107:3864–3869

RABBITT RD, BRICHTA AM, TABATABAEE H, BOUTROS PJ, AHN JH, DELLA SANTINA CC, POPPI L, LIM R. (2016) Heat pulse excitability of vestibular hair cells and afferent neurons. J Neurophysiol. 2016 May 25:jn. 00110

RAJGURU SM, RICHTER C-P, MATIC AI, HOLSTEIN GR, HIGHSTEIN SM, DITTAMI GM, RABBITT RD (2011) Infrared photostimulation of the crista ampullaris. J Physiol 589:1283–1294

RAPRAEGER A (1989) Transforming growth factor (type beta) promotes the addition of chondroitin sulfate chains to the cell surface proteoglycan (syndecan) of mouse mammary epithelia. J Cell Biol 109:2509–2518

SALIBA M, RAMALANJAONA N, GULBERTI S, BERTIN-JUNG I, THOMAS A, DAHBI S, LOPIN-BON C, JACQUINET JC, BRETON C, OUZZINE M, FOURNEL-GIGLEUX S (2015) Probing the acceptor active site organization of the human recombinant β1,4-galactosyltransferase 7 and design of xyloside-based inhibitors. J Biol Chem. 2015. Mar 20 290(12):7658–7670

SANTI PA, ANDERSON CB (1986) Alcian blue staining of cochlear hair cell stereocilia and other cochlear tissues. Hear Res 23:153–160

SCHRADERS M ET AL. (2012) Mutations of the Gene encoding otogelin are a cause of autosomal-recessive nonsyndromic moderate hearing impairment. Am J Hum Genet 91:883–889

SCHWARTZ NB, GALLIGANI L, HO PL, DORFMAN A (1974) Stimulation of synthesis of free chondroitin sulfate chains by beta-D-xylosides in cultured cells. Proc Natl Acad Sci U S A 71:4047–4051

SILVER RB, REEVES AP, STEINACKER A, HIGHSTEIN SM (1998) Examination of the cupula and stereocilia of the horizontal semicircular canal in the toadfish *Opsanus tau*. J Comp Neurol 402:48–61

SIMMLER MC, COHEN-SALMON M, EL-AMRAOUI A, GUILLAUD L, BENICHOU JC, PETIT C, PANTHIER JJ (2000) Targeted disruption of otog results in deafness and severe imbalance. Nat Genet 24:139–143

SUGIYAMA S, SPICER SS, MUNYER PD, SCHULTE BA (1991A) Histochemical analysis of glycoconjugates in gelatinous membranes of the gerbil's inner ear. Hear Res 55:263–272

SUGIYAMA S, SPICER SS, MUNYER PD, SCHULTE BA (1991B) Distribution of glycoconjugates in ion transport cells of gerbil inner ear. Journal of Histochemistry & Cytochemistry 39:425–434

SUZUKI H, KATORI Y, TAKASAKA T (1996) Carbohydrate composition of stereociliary glycocalyx of the utricle of guinea pig inner ear. Acta Otolaryngol 116:12–16

TAKUMIDA M (2001) Functional morphology of the crista ampullaris: with special interests in sensory hairs and cupula: a review. Uchū Seibutsu. Kagaku 15:356–358

TAKUMIDA M, WERSÄLL J, BAGGER-SJÖBÄCK D (1989A) Sensory hair fusion and glycocalyx changes after gentamicin exposure in the guinea pig. Acta Otolaryngol Suppl 457:78–82

TAKUMIDA M, HARADA Y, BAGGER-SJÖBÄCK D, WERSÄLL J (1989B) Carbohydrates of the guinea pig vestibular supporting cells. Auris Nasus Larynx 16:133–142

TAKUMIDA M, BARBARA M, BAGGER-SJÖBÄCK D, RASK-ANDERSEN H (1989C) Lectin detection of carbohydrates in the endolymphatic sac. Archives of oto-rhino-laryngology 246:89–93

TAUBER R, REHER K, HELLING K, SCHERER H (2001) Complex carbohydrates—structure and function with respect to the glycoconjugate composition of the cupula of the semicircular canals. Biological Science in Space:362–366

TORIHARA K, MORIMITSU T, SUGANUMA T (1995) Anionic sites on Reissner's membrane, stria vascularis, and spiral prominence. The journal of histochemistry and cytochemistry: official journal of the histochemistry. Society 43:299–305

TRAN VM, VICTOR XV, YOCKMAN JW, KUBERAN B (2010) RGD-xyloside conjugates prime glycosaminoglycans. Glycoconj J 27:625–633

TSUPRUN V, SANTI P (2001) Proteoglycan arrays in the cochlear basement membrane. Hear Res 157:65–76

WEINSTEIN T, EVRON Z, TREBICZ-GEFFEN M, AVIV M, ROBINSON D, KOLLANDER Y, NEVO Z (2012) β-D-xylosides stimulate GAG synthesis in chondrocyte cultures due to elevation of the extracellular GAG domains, accompanied by the depletion of the intra-pericellular GAG pools, with alterations in the GAG profiles. Connect Tissue Res 53(2):169–179

YARIZ KO ET AL. (2012) Mutations in OTOGL, encoding the inner ear protein otogelin-like, cause moderate sensorineural hearing loss. Am J Hum Genet 91:872–882